Optical Materials 126 (2022) 112215

Contents lists available at ScienceDirect

Optical Materials

journal homepage: www.elsevier.com/locate/optmat

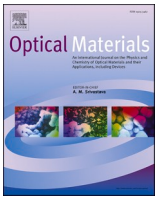

Effect of annealing temperature on the structural, thermoluminescent, and optical properties of naturally present salt from Lluta region of Peru

Carlos D. Gonzales-Lorenzo [a,b,*], Darwin J. Callo-Escobar [a,**], Alberto A. Ccollque-Quispe [a], T. K. Gundu Rao [a], F.F.H. Aragón [a], J.C.R. Aquino [a], D.G. Pacheco-Salazar [a], H. Loro [c], Jose F. Benavente [d], Jessica Mosqueira-Yauri [a], Henry S. Javier-Ccallata [a], Jorge S. Ayala-Arenas [a], Nilo F. Cano [e]

[a] Universidad Nacional de San Agustín (UNSA), Av. Independencia S/N, Arequipa, Peru
[b] Instituto de Física, Universidade de São Paulo, Rua do Matão, Travessa R, 187, CEP 05508-090, São Paulo, SP, Brazil
[c] Faculty of Sciences, National University of Engineering, Lima, Peru
[d] CIEMAT, Av, Complutense 40, E-28040, Madrid, Spain
[e] Instituto do Mar, Universidade Federal de São Paulo, Rua. Doutor Carvalho de Mendonça, 144, CEP 11070-100, Santos, SP, Brazil

ARTICLE INFO

Keywords:
Halite (NaCl)
Anhydrite ($CaSO_4$)
Structural properties
Optical band gap energy
Thermoluminescence (TL)

ABSTRACT

The effect of annealing temperature on the structural, thermoluminescence, and optical properties of the thermally treated naturally occurring salt from Lluta were studied. Samples were submitted to different annealing temperatures from 300 to 700 °C for 30 min. X-ray diffraction analysis of all samples was performed. The predominant crystalline phase found in the Lluta salt sample is NaCl, with minor phases ($CaSO_4$ and Na). TL technique has been used to characterize and determine the dosimetric properties. After the thermal annealing process of samples, an increase in the TL response of up to 80 times the TL intensity of the natural sample is observed. A promising dosimetric high-temperature peak was found for the sample with an annealing temperature of 400 °C for 30 min. Besides, activation energy, frequency factor, and peak position have been determined by E-Tstop, Tm-Tstop, and deconvolution methods. The UV–Vis optical absorption of Lluta salt sample subjected to several annealing temperatures was investigated. The optical energy gap Eg was calculated using the Tauc relation and the relation between the variation of the optical band gap and the density of thermoluminescent traps was analyzed.

1. Introduction

As can be seen today, the use of different types of radiation is becoming widespread in various human activities, such as the intensive development of radiation technologies, testing, sterilizing, and processing materials [1–3]. As a consequence, accidents involving nuclear radiation could occur near nuclear plants or where ionizing radiation sources are employed for different purposes [4–8]. In these cases, undesired emitted radiation can accidently affect the nearby population being dangerous to human health. Nowadays a nuclear accident is unlikely due to the all extensive protection and highly controlled system securities considered before the design of the nuclear facility. However, prevention is always the best way to be ready for unexpected accidents. Therefore, the use of ionizing radiation, which is carcinogenic, must always be associated with an efficient radiological protection system as a means of safety. In this sense, the use of dosimeters is widely used as radiation detectors to monitor people who often work with radiation sources in medical centers or nuclear facilities. Among them, luminescence materials as a good alternative to passive detectors for radiation dose measurement have been studied for decades [1,9–11].

Retrospective and emergency dosimetry are known because their study is based on an immediate and long-term determination, respectively, of the absorbed dose by populations and individuals due to a radiation accident resulting in possible leakage of radiation emission to the environment beyond normal background radiation [12–18]. Since synthetic dosimeter is not always available in place at the time of a

* Corresponding author. Universidad Nacional de San Agustín (UNSA), Av. Independencia S/N, Arequipa, Peru
** Corresponding author.
E-mail addresses: cgonzaleslo@unsa.edu.pe (C.D. Gonzales-Lorenzo), dcallo@unsa.edu.pe (D.J. Callo-Escobar).

https://doi.org/10.1016/j.optmat.2022.112215
Received 14 December 2021; Received in revised form 1 March 2022; Accepted 8 March 2022
Available online 16 March 2022

possible nuclear disaster, researchers have chosen on finding locally available materials that can be used as luminescence materials for the determination of the absorbed dose [19].

Among the investigated materials, there are integrated circuits (ICs) from several mobile phones [20,21], mobile phone protective touchscreen glass [22,23], SMD resistors [24], silicates contained in dust [25], natural silicate [26,27] and natural halite (NaCl) [17].

Natural sodium chloride (NaCl) also known as mineral Halite has been widely studied in the past due to its high sensitivity shown for ionizing radiation, relatively easy presence of this mineral in almost every home around the world (household salt), and very low cost [12, 14,16–18,28]. As a result, natural or synthetic NaCl (pure and doped form) has been especially focused for their use in retrospective dosimetry as a passive dosimeter due to its high sensitivity to gamma [12–14, 17,18,28,29] and beta radiation [15,30,31]. Thermoluminescence (TL), optically stimulated luminescence (OSL), optical absorption (OA), photoluminescence (PL) are the main techniques used for this purpose [12-15, 28–32]. Natural mineral of NaCl extracted from different localities around the world has been obtained and their luminescence properties analyzed for retrospective and emergency dosimetry purposes. Among them, we have natural salt from the Dead Sea whose study is adopted as a model thermoluminescence dosimetry system [16]. Natural salt extracted from the Seawater of the Mediterranean Sea has been characterized by the TL technique for determining dosimetric properties [15,17] have studied the TL sensitivity of Egyptian halite (NaCl) samples for potential application in retrospective dosimetry. Besides, Israeli salt samples (NaCl) were exposed to gamma radiation dose from 0.5 mGy to 300 Gy using a calibrated ^{137}Cs source to examine the potential use of these samples in retrospective dosimetry (RD) [18]. Finally, Ekendahl et al. [33] have investigated the potential use of NaCl in the form of a household salt from Czech Republic as a retrospective and accident dosemeter using the OSL technique.

On the other hand, Pearse et al. [34] have found that the principal impurity found in naturally occurring rock salt is calcium sulfate, generally 1–4%, with small amounts of calcium chloride and magnesium chloride. In the United States, for instance, bedder deposits of salt formation showed layers of halite (NaCl) separated by layers of anhydrite ($CaSO_4$), besides other mineral impurities that including shale, iron pyrites, and silica [35]. Sodium chloride appears as a white crystalline solid. However, it can show different colors, such as white, gray, reddish, or even brownish. The color can be attributed to impurities present in the sample, such as Mg, Mn, K, Li, Cu, either occluded or on the surface of the crystals [35,36]. Sonnenfeld et al. [37] have done an extensive study of the different natural occurrences that provoke discolored pure rock salt. Essentially, colorless halite is discolored by interstitial admixtures, or by colloids inserted into structural defects of the crystal lattice. Orange color, for instance, is produced by traces of sylvite particles 150–180 nm [37].

In this sense, the use of materials available in nature is of great importance due to their availability and their high sensitivity to ionizing radiation. Such is the case of the Sal of Lluta, which is widely used by the population of the Lluta region in Arequipa, Peru. This material in grains has shown high sensitivity to gamma radiation, which makes its study as an ionizing radiation dosimeter of great interest. Furthermore, further studies would include the use of Lluta salt samples not only as gamma detectors but also as UV radiation detectors, given the high UV index present in this southwestern region of Peru. The present work will focus on investigating the natural salt from the Lluta region in Peru by TL technique and UV–Vis absorption for their possible application in radiation dosimetry.

Furthermore, thermal annealing of samples is a technique used by several authors in order to improve their luminescence properties [28, 38]. In many cases, the thermal annealing on the samples shows a significant improvement and an optimal luminescent response to continue their studies as dosimetric material. However, a comprehensive analysis of heat treatments' effect on the crystal structure, thermoluminescent kinetics, and optical properties are not properly carried out. In this work, the salt from Lluta obtained naturally was crushed and subjected to different annealing temperature conditions. The effect of different annealing temperatures (AT) on its thermoluminescence properties has been analyzed within a wide range of gamma radiation doses. Furthermore, the effect on the phase concentration, lattice constant, and full width at half maximum (FWHM) were performed after different AT. Finally, UV–Vis absorption spectra of natural as-collected and thermal annealing samples were performed and the optical band gap energy was analyzed.

2. Experimental details

a) *Collection:* Natural rock salt used in this study was extracted from the mines of Lluta district, Arequipa region, Peru. Lluta mines are located in the Arequipa region southern Peru (15°58′07.8"S latitude, 71°59′30.9"W longitude) as can be seen in Fig. 1(a). Fig. 1(b) shows the natural rock salt from Lluta. The salt sample was crushed and sieved to retain grains of 90–150 μm in size for TL measurements, while grains smaller than 75 μm in diameter were used in structural X-ray diffraction (XRD) analysis.

b) *Thermal annealing:* For thermal annealing of samples, a high-temperature oven, model VECSTAR, which operates at a temperature of 900 °C was used. Firstly, thermal annealing of samples in grain size (90–150 μm) were carried out at different temperatures at 300, 350, 400, 450, 500, 600, and 700 °C for 30 min. TL, XRD, and optical absorption analyses were performed on these samples. Additionally, these grains, of the same size, were subjected to 400 °C of AT. Samples were maintained in this condition for 30 min, 1h, 2h, 4h, 6h, 8h, 12 h, and 24 h, after that, removed from the oven and placed at room temperature.

c) *XRD analysis:* A commercial X-ray diffractometer (Rigaku Miniflex 600) equipped with CuKα radiation was used to assess the crystal structure and estimate the grain size of the natural Lluta salt and those with annealing temperatures (AT). X-ray diffraction (XRD) data in the range of $20° \leq 2\theta \leq 80°$, with steps of 0.02°, were recorded. The XRD patterns were analyzed with the Rietveld refinement method using the GSAS (General Structure Analysis System) software within the EXPGUI interface [39,40].

d) *Thermoluminescence:* The irradiations for TL measurements were carried out at the Professional School of Physics of UNSA (EPF-UNSA) using a Co-60 source from Picker, model Gammatron with a dose rate of 97.3 mGy/min at 10 cm from the source. The γ-irradiation was performed at room temperature and under conditions of electronic equilibrium. After irradiation samples of Lluta salt were kept in the dark until TL measurements. Harshaw TL reader model 3500 in a nitrogen atmosphere was used for the TL measurements; equipped with a photomultiplier tube (PMT) for light detection. The heating rate was kept at 4 °C/s. Five TL reading measurements were carried out to obtain an average TL glow curve. All TL readings were carried out 2 weeks after the irradiation took place, time enough to reach the stability of the TL peaks in the Lluta salt sample, except for the study of the fading of TL peaks at room temperature.

e) *Optical absorption:* UV–Vis spectra were collected using a Shimadzu UV-1800 spectrophotometer operating in the region from 190 to 1100 nm, with the detector at the absorption position. The UV–Vis absorption spectra of Lluta salt samples treated at different AT were weighed with 3 mg and shaken with 3 ml of distilled water before each measurement.

3. Results and discussion

3.1. X-ray diffraction results

Fig. 2 (a) shows the XRD patterns (open black symbols) of the natural as-collected and thermal annealed Lluta salt, where the intensity is

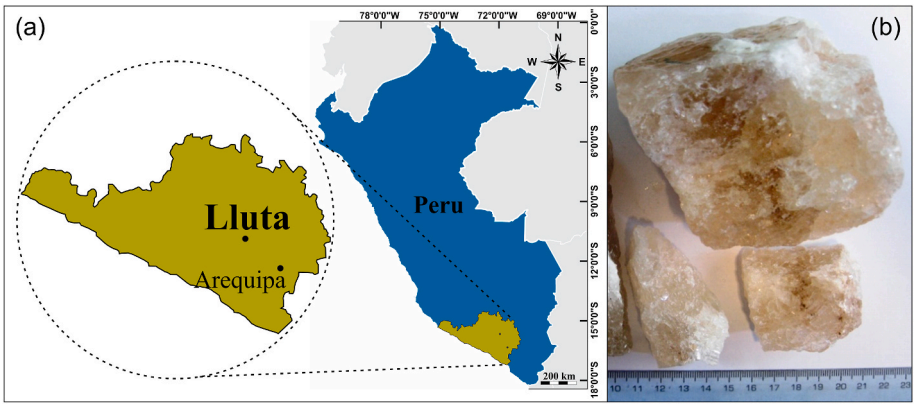

Fig. 1. (a) Lluta district location. (b) Natural rock salt from Lluta region.

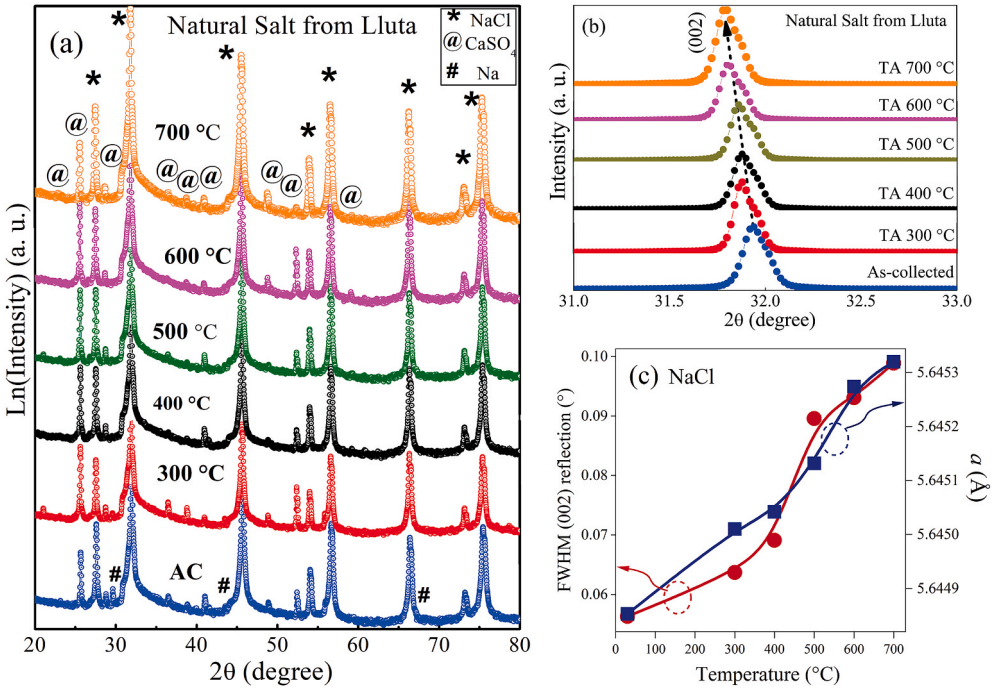

Fig. 2. (a) XRD patterns of Lluta samples treated at different temperatures. The peaks marked with *, @, and # have been associated with the halite (NaCl), anhydrite ($CaSO_4$), and Na crystalline phases, respectively. (b) Magnification, and (c) FWHM, and lattice constant of (002) peak as a function of temperature.

plotted on a logarithmic scale to visualize the secondary phases, within the sensitivity limit of the instrument. The diffraction peaks marked with (*) in the spectrum are in agreement with the crystalline halite (NaCl) cubic phase (with space group: Fm-3m), which is identified from its main reflections (002), and (022) located at 31.9°, and 45.7°, respectively, as well as the less intense peaks (111), (113), (222), (004) and (024). The formation of anhydrite ($CaSO_4$) orthorhombic crystalline phase (with space group: Amma) was identified from its main reflection Bragg peak (@) (200) located at 25.66°. Following, a crystalline phase of sodium (Na) is observed only in low-temperature thermal annealing (300 °C) and in samples as collected (AC), which is identified by the peak located at (#) ~30°, suggesting that the thermal treatment induces the migration of these clusters to the NaCl phase. For all recorded XRD patterns, Rietveld refinements were performed to access structural parameters such as phase concentration, lattice constant, and full width at half maximum (FWHM). An example refinement is shown in Fig. 3, where the symbols (spheres) represent experimental data, the solid red line represents calculated data and the lower blue line represents the difference between them.

Fig. 2 (b) exhibits a shift to lower angles of the main peak 002 suggesting an increase of the lattice constant, this tendency is quantified and it is shown in Fig. 2 (c) where the lattice increase from 5.6449(1) Á to 5.6453(1) Á. These values are in agreement with the experimental NaCl bulk lattice constant, 5.64 Å measured at 293 K [41]. Concerning the FWHM as it is displayed in Fig. 2(c), it exhibits an increase in the thermal annealing, confirming the improvement of crystallinity as the thermal annealing.

Consequently, the predominant crystalline phase is NaCl, with minor phases ($CaSO_4$ and Na) accounting for less than 5% of the total.

3.2. Thermoluminescence studies

a) In the first place, TL glow curves of all samples with a previous AT from 300 to 700 °C for 30 min and irradiated with a gamma dose of 2 Gy (Co-60) are shown in Fig. 4. The gamma irradiation dose of 2 Gy was chosen to avoid a supralinear dose. As can be seen in Fig. 4, TL glow curves with AT namely 300, 350, and 400 °C for 30 min show a prominent TL peak at around 272 °C. For the TL glow curves

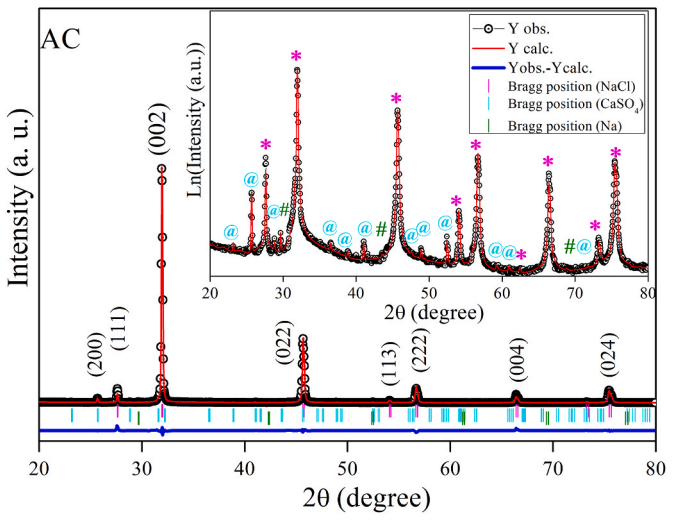

Fig. 3. Rietveld refinement of the salt from Lluta region, as-collected. The symbols (spheres) represent the experimental data, while the solid red line represents the calculated data and the lower blue line represents the difference between them. The inset figure shows the refinement with the Y-axis on a logarithmic scale. (For interpretation of the references to color in this figure legend, the reader is referred to the Web version of this article.)

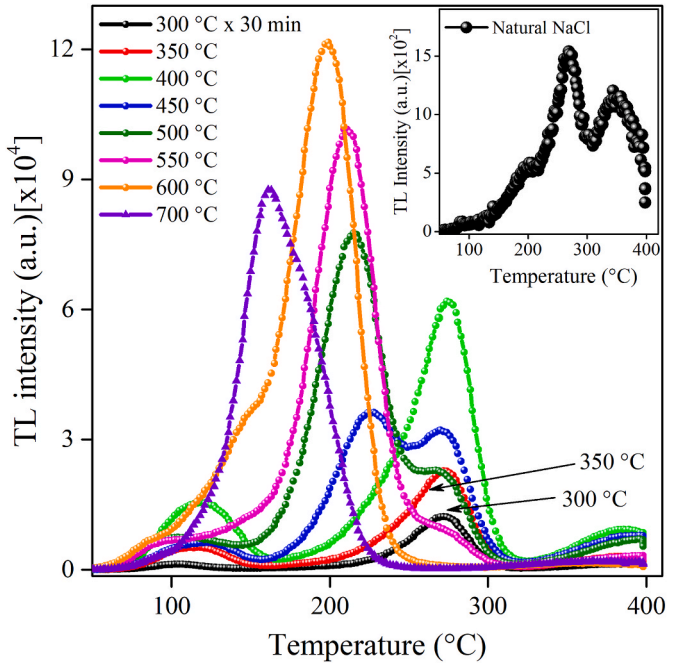

Fig. 4. TL glow curves of Lluta salt samples with previous AT from 300 to 700 °C and irradiated at 2 Gy of gamma dose from a Co-60 source. In the inset of the figure, the TL glow curve of the natural salt from Lluta (as collected) for 2Gy of dose irradiation is shown. In all cases, a mass of about 8.4 mg was used.

corresponding to an AT of 450, 500, and 550 °C for 30 min, TL peak around 272 °C decreases, and another peak of greater intensity appears at lower temperatures. For the sample corresponding to an AT of 450 °C for 30 min, a TL peak of greater intensity around 224 °C can be seen. For the case of an AT of 500 °C for 30 min, the TL peak of greatest intensity appears at about 215 °C. For the case of 550 °C for 30 min, a maximum TL peak appears at about 211 °C. Finally, for the samples corresponding to an AT of 600 °C and 700 °C for 30 min, prominent TL peaks at about 199 °C and 161 °C, can be seen, respectively. The mass used in the measurements was approximately 8.4 mg. Each TL glow curve represents the average of 5 measurements. The inset of Fig. 4 shows in more detail the TL curve of the natural salt of Lluta as collected and irradiated at 2 Gy of gamma radiation dose. This curve shows a low-intensity TL peak around 206 °C, a prominent TL peak around 269 °C, and a high-temperature TL peak at about 350 °C.

A similar study has been made by Khazal and collaborators [38]. These authors have studied the food salt as a gamma radiation dosimeter. They have found that previous pre-irradiation annealing at 400 1C/h, 100 °C/2 h increases the salt sensitivity and the post-irradiation annealing with 100 °C/20 min reduces the thermal fading. Furthermore, Amer [28] has presented the TL characteristics of the thermally treated household NaCl. In this study, the salt sample was subjected to a heating rate of 10 °C/min and kept for 1 h at different annealing temperatures namely, 200, 300, 400, 500, and 600 °C respectively. As a result, TL response was enhanced as the annealing temperature increases displaying a maximum response at 500 °C and then drops afterward.

Among those glow curves shown in Fig. 4, the curve of greatest interest is that with an AT of 400 °C for 30 min because it presents a prominent peak at the highest temperature (at about 272 °C), keeping in mind its possible use in dosimetry radiation.

It is worth noting that increasing annealing temperatures in the sample indicate an increase in the lattice constant as shown in Fig. 2(c). This increase could promote the appearance of both deep and shallow TL traps. This can be seen from the fact that after the thermal annealing process samples had a significant improvement in the TL intensity as can be seen in Fig. 4. For example, after an AT of 400 °C for 30 min, the TL intensity had an increase of about 40 times the TL intensity of the natural sample (as collected). In the case of an AT of 600 °C for 30 min, there was an increase in TL intensity of about 80 times more than the TL response of the collected sample. This analysis will be seen in more detail later.

b) In the second place, samples in grains form were subjected to an AT of 400 °C. Samples were maintained at this temperature for different times from 0.5 to 25 h and irradiated with 2 Gy of gamma radiation dose.TL glow curves of these samples are shown in Fig. 5. For cases corresponding to an annealing time of 30 min and 1 h, a TL peak of greater intensity is observed at about 270 °C (Fig. 5(a)). As the annealing time at 400 °C increases (from 2 to 24 h), the TL peak around 270 °C decreases until it completely disappears, and at the same time, a prominent TL peak at about 224 °C appears as can be seen in Fig. 5.

The intensity of the TL peak at 224 °C was monitored as a function of time with the sample kept at 400 °C. The resulting annealing behavior of this TL peak is shown in the inset of Fig. 5(b). As can be seen in this figure, the TL intensity has an increasing behavior up to a saturation point at a time of 12 h and then it decreases for a longer annealing time.

On the basis of this observation, the sample that was annealed for 8 h at 400 °C was selected for further studies. An interesting observation is that for a thermal anneal for 30 min, a high temperature TL peak is observed.

c) Fading: an important property of any TL material is the fading of TL intensity with time [42]. Lluta sample with previous thermal annealing of 400 °C for a time of 30 min and 8 h were irradiated at 2 Gy of gamma radiation dose and kept in the dark. Its TL was read out after, 0.28, 0.52, 2.73, 5.05, etc. h up to about 39 days. The result is shown in Fig. 6. Firstly, Fig. 6(a) shows the fading of TL glow curves of the Lluta sample, with a previous AT of 400 °C for 30 min, after different storage times. These glow curves show TL peaks at about 100 °C, a prominent peak at 267 °C, and finally a low TL peak at about 360–370 °C. Secondly, Fig. 6(b) shows the fading of TL glow

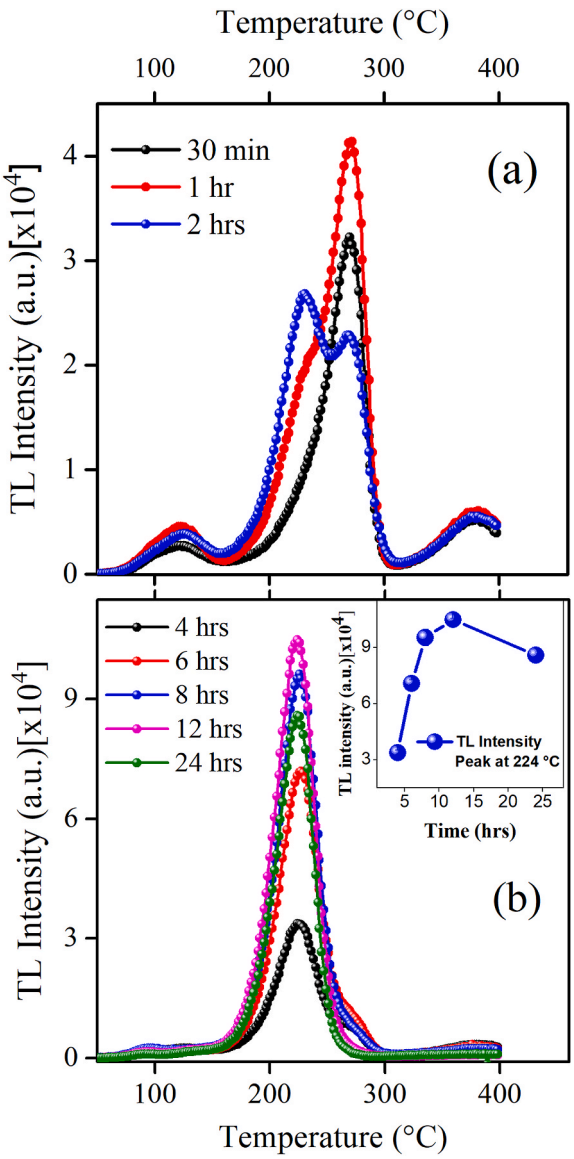

Fig. 5. TL glow curves of Lluta salt samples at different times of an AT of 400 °C and irradiated at 2 Gy of gamma radiation dose (a) from 30 min to 2 h, and (b) from 4 to 24 h. In all cases, a mass of about 8.4 mg was used. The inset of Fig. 5 (b) shows the maximum intensity of the TL peak at about 224 °C as a function of the thermal annealing time.

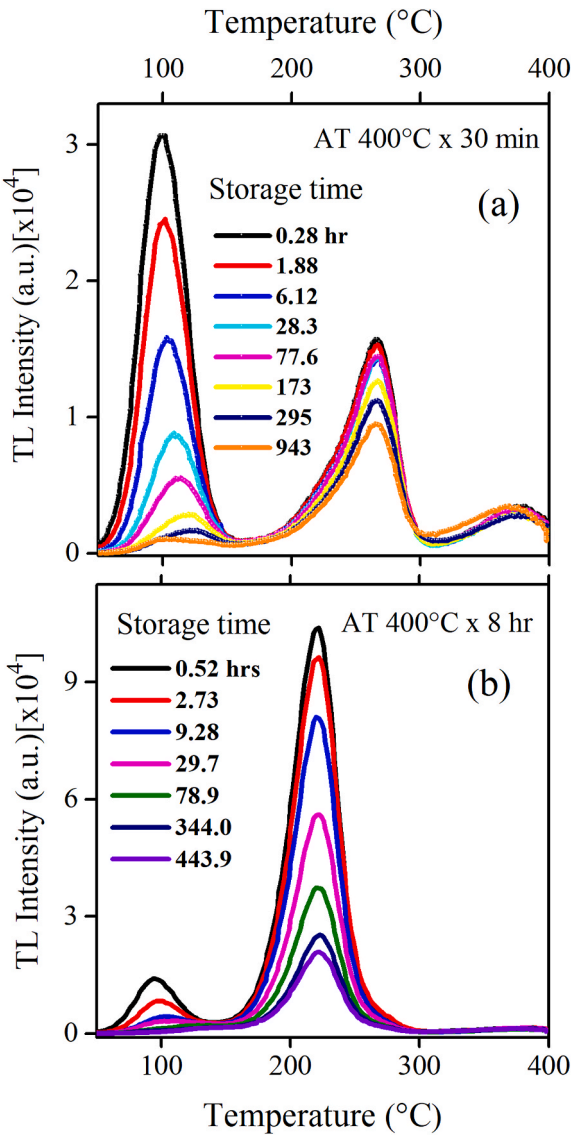

Fig. 6. TL glow curves of the natural sample of salt from Lluta irradiated at 2Gy dose at different storage times. The upper and lower figures correspond to the sample with an AT of 400 °C (a) for 30 min and (b) for 8 h, respectively.

curves of the Lluta sample, with a previous AT of 400 °C for 8 h, after different storage times. In this case, these glow curves show their main TL peaks at about 100 and 222 °C.

Fig. 7 shows the fading of 224 °C TL peak corresponding to the sample with an AT of 400 °C for 8 h. Analyzed time was performed from 0.5 to 440 h. In this figure, it is observed that after approximately 79 h (3.3 days) the TL intensity decreases by about 64.1% of the initial TL intensity. After that, the fading has a negative slope linear behavior up to 444 h (18.5 days). In this sense, the continuous fading of the TL peak makes its use in dosimetry not possible.

Additionally, Fig. 8 shows the fading of 100 and 269 °C TL peaks corresponding to the sample with an AT of 400 °C for 30 min. Analyzed time was performed from 0.28 to 943 h. It is observed that for the 100 °C TL peak, after approximately 437 h (~18 days), TL intensity drops about 96% of the initial TL intensity. For the TL peak around 269 °C after approximately 437 h (~18 days) the TL intensity drops about 35% from the initial TL intensity. After that, fading has a constant behavior up to 943 h (~39 days). Hence, between 18 and 39 days after the exposure, in order to avoid fading effects, fading characteristics of the mentioned TL peak of the Lluta sample make possible its use in retrospective dosimetry.

d) Dose-response curve: furthermore, samples with an AT of 400 °C for 30 min were irradiated with doses higher than 50 mGy. These TL glow curves show a low-temperature peak at about115–130 °C and a prominent 270 - 276 °C TL peak as can be seen in Fig. 9. Fig. 9(a) shows TL glow curves of samples irradiated with low doses between 5 mGy and 100 mGy. Fig. 9(b) shows the TL glow curves of samples irradiated with gamma radiation with doses from 200 mGy to 5Gy. These results show that a natural sample with previous thermal annealing of 400 °C for 30 min is a very sensitive ionic crystal as far as its thermoluminescence is concerned and to a wide range of gamma radiation dose, from 50 mGy to 5 Gy. Fig. 10 shows the TL response of the main TL peak at 270 - 276 °C for doses ranging from mGy to Gy range. Analyzing the dose-response curves with log axes, as can be seen in Fig. 10, the TL response of peak at 270 - 276 °C has a linear behavior, with a linear equation: $I_{TL} = 1.390*Dose + 0.683$ in

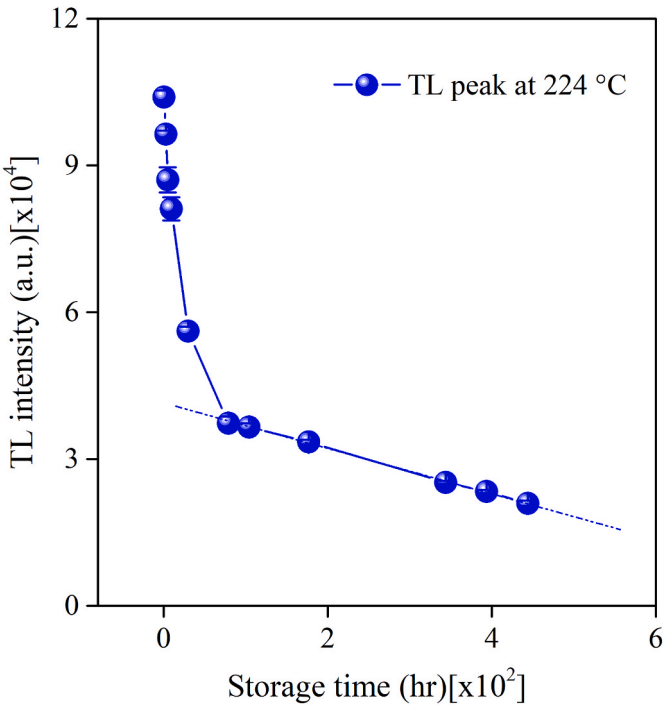

Fig. 7. TL intensity of the Lluta salt sample with an AT of 400 °C for 8 h, irradiated with 2 Gy of gamma radiation against the storage time at room temperature. TL peak corresponds to that of 224 °C.

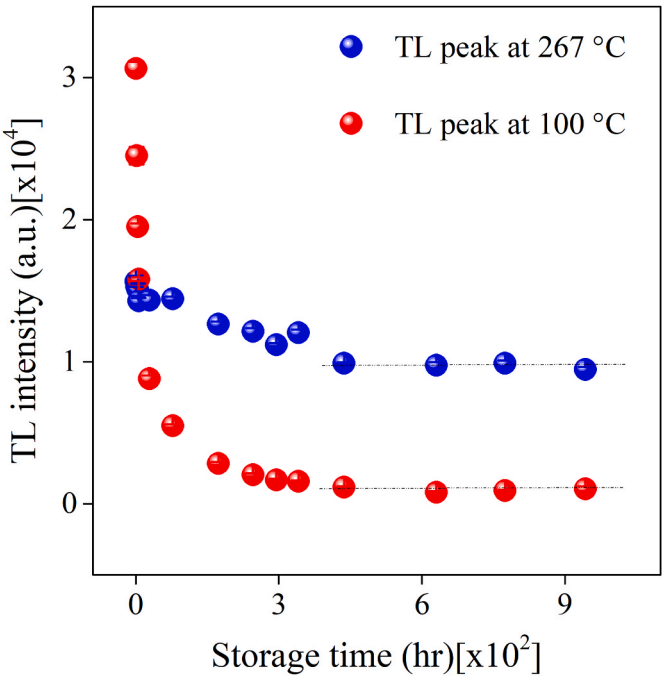

Fig. 8. TL intensity of the Lluta salt sample irradiated with 2 Gy of gamma radiation dose against the storage time at room temperature. Sample with an AT of 400 °C for 30 min and TL peaks correspond to that of 100 and 267 °C.

the dose range from 50 mGy up to 5 Gy. As a consequence, Lluta salt in grains form can be properly used as a gamma detector in the range of 50 mGy to a few Gy.

e) Deconvolution: the number and position, as well as the activation energy and frequency factor of the TL peaks contained in the experimental complex glow curve of the sample with an AT of 400 °C for 30 min, were determined by the E-Tstop [43], T_M-Tstop [44] and deconvolution [45] methods. The E-Tstop method used to calculate the activation energy of the traps is based on the initial rise method. In this method, the initial part of the TL glow curve can be well described by an exponential behavior such as exp(-*E*/kT). Later, by the Arrhenius plot: ln(TL) vs 1/T which will be approximated as a straight line. After this approximation, the activation energy *E* can be easily obtained from the slope -*E*/*k*. For a reliable result, it is only considered below 15% of the maximum TL intensity [46]. In this work, the activation energy was found using different preheating temperatures (Tstop) from 50 to 300 °C at a 5 °C scanning step. The obtained activation energies (*E*) using the E-Tstop method as a function of the Tstop is displayed in Fig. 11.

The TL glow curve of the sample with an AT of 400 °C/30min after gamma irradiation of 2 Gy (Fig. 9(b)) is dominated by peaks at about 120 °C, 272 °C, and 375–380 °C. These TL glow curves are generally composed of several overlapping glow peaks. The deconvolution method is a convenient tool to obtain the number and position as well as the activation energy and frequency factor of all the peaks without any

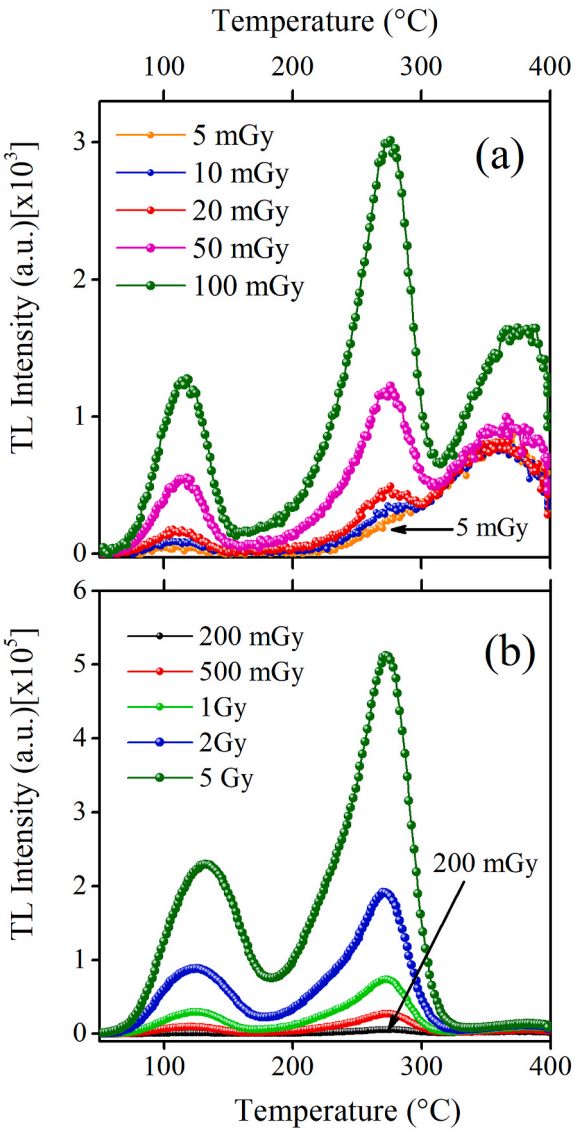

Fig. 9. TL glow curves of Lluta salt sample with an AT of 400 °C for 30 min irradiated with low gamma radiation doses of (a) 5 mGy up to 100 mGy and of (b) 200 mGy up to 5 Gy using a mass of about 8.6 mg. (b) TL glow curves of samples irradiated with gamma radiation doses (Co-60 source).

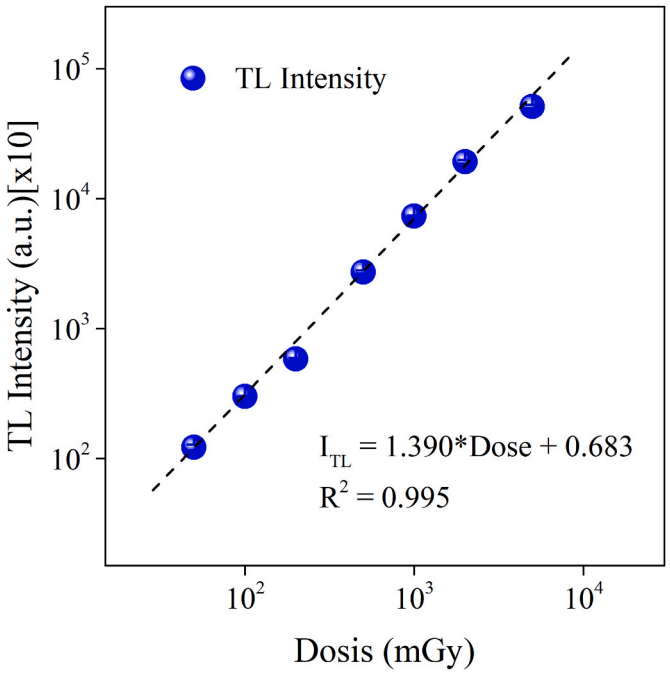

Fig. 10. TL intensity behavior of the 270–276 °C TL peak shown in Fig. 9, as a function of gamma radiation doses, the dashed line indicates linearity.

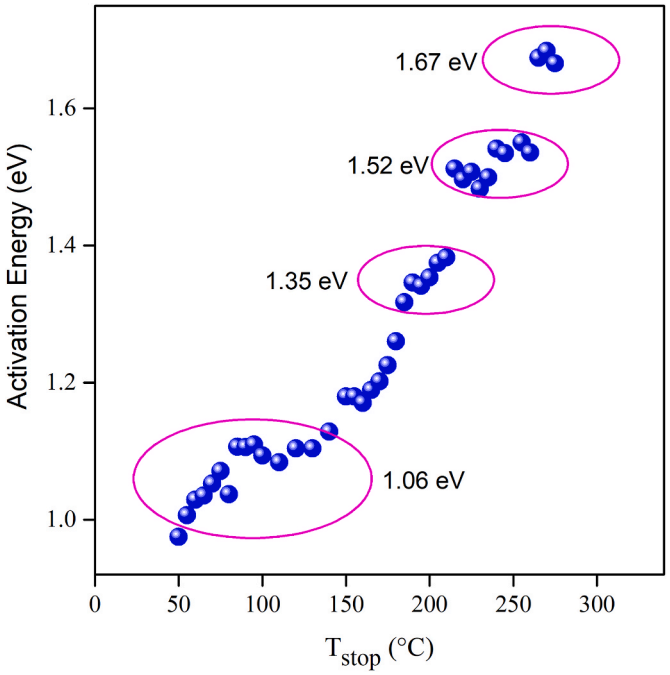

Fig. 11. Activation energy vs. Tstop method.

additional experimental repetition. However, before applying the deconvolution method, some information on the number of superimposed glow peaks is necessary. For this preliminary analysis of the number of TL peaks, the Tm-Tstop method [44] was used.

Fig. 12 shows the first maximum temperatures T_M of the remaining TL glow peaks corresponding to each Tstop temperature following the T_M-Tstop method. With the above result, it is possible to estimate the number of individual TL curves in which our experimental TL glow curve is composed. There are apparently three plateau regions, which indicate that the emission of the TL glow curve of the salt sample consists

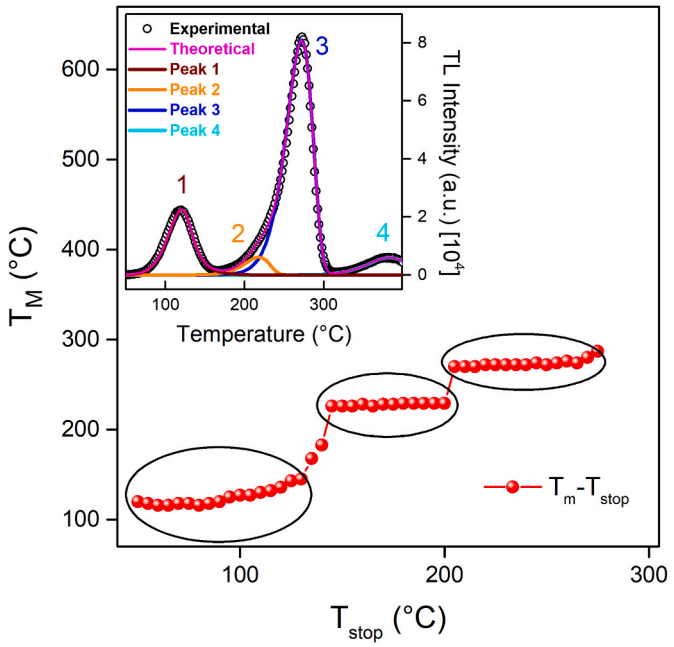

Fig. 12. Tm vs. Tstop. In the inset, TL glow curve of the Lluta salt sample with an AT of 400 °C for 30 min, irradiated with gamma dose of 2 Gy. A good fit between the experimental glow curve (black circles) and the theoretical glow curve (pink line) can be achieved assuming the presence of four peaks. (For interpretation of the references to color in this figure legend, the reader is referred to the Web version of this article.)

of at least three glow peaks.

The experimental TL glow curve was fitted using deconvolution methods (see in the inset of Fig. 12), implemented in a software tool that resolves every experimental curve in individual glow peaks. Thus, to get the kinetic parameters; a mathematical model based on four functions was used considering the previous results of T_M-Tstop and E-Tstop. The first three related to the first-order kinetics (F.O.K.) approach using continuous trap distribution and the last one with a discrete of trapping centers based on general order kinetics, according to the results of the Tm-Tstop. As a result, four computed TL peaks at about 120 (peak 1), 216 (peak 2), 269 (peak 3), and 379 °C (peak 4) were found. For the peaks arising from a continuous distribution of trapping centers, an exponential function can be considered, as follow:

$$n(E) = \frac{n_0}{\sigma} e^{-\frac{E-E_0}{\sigma}} \quad (1)$$

Both σ parameters related to the second and the third contribution are low enough that the shapes of these continuous distributions are similar to discrete distributions. In addition, the last contribution shows electron re-entrapment related to the general order kinetics (G.O.K.) approach. Which are in agreement with the results of E-Tstop. Quality of fit was tested with the Figure of Merit (FOM = $\sum(TL_{exp} - TL_{comp})/TL_{comp}$) [47]. FOM = 2.57% shows that data fit is satisfactory. Kinetic order, the position of the maximum temperature (T_M), activation energies (E), and frequency factor (s) of TL peaks of the Lluta sample are shown in Table 1. First and general kinetic order are represented as F

Table 1
Kinetic order, maximum temperature (T_M), activation energy (E), and frequency factors (s) for each deconvolved peak in the TL glow curve.

Peak	Order	T_M (°C)	E (eV)	s (s^{-1})
1	F	120	1.06	1.23×10^{13}
2	F	216	1.35	2.13×10^{13}
3	F	269	1.52	3.24×10^{13}
4	G	379	1.67	1.47×10^{12}

and G respectively. The results of the activation energy obtained by the E-Tstop analysis compared with the values obtained by the deconvolution method are in good correlation with each other. The frequency factor of the deconvoluted peaks was calculated according to Eq. (3) [48].

$$s = \frac{\beta E}{kT_m^2}\exp\left(\frac{E}{kT_m}\right) \quad (2)$$

3.3. UV–visible absorption spectroscopy

UV–Vis absorption spectra of natural as-collected and thermal annealing samples (from 300 to 700 °C for 30 min) were carried out as it is shown in Fig. 13. Absorbance spectra of all samples exhibit broadband between 190 and 212 nm which is attributed to charge transfer transition in the crystal structure of the NaCl compound as is suggested by Gopikrishnan et al. [49], which have been shown that alkali-halide compounds are wide band gap insulators, that explains their optical transparency. Beyond 205 nm, no absorption bands are observed. It shows that the Lluta salt sample is transparent in the visible region with a band absorption in the UVC region.

The optical band gap energy (Eg) of the Lluta salt samples with different AT were calculated using the Tauc relation [50], shown in Eq. (3).

$$(\alpha h\nu)^n \sim (h\nu - E_g) \quad (3)$$

where $h\nu$ is the photon energy, α is the optical absorption coefficient near the fundamental absorption edge, and n = 2 for a direct transition and n = 1/2 for an indirect transition [51]. Kiran Kumar et al. [52], and Ali Ahmed et al. [53] have based their studies on samples based on NaCl compounds. They have shown the optical band gap energies Eg calculated using the Tauc plot method for both cases the direct and indirect transition. The values shown in these studies indicate a slightly higher value of the optical band gap for the case of the direct transition compared to the indirect transition.

Fig.14(a) and (b) display the curves of $(\alpha h\nu)^n$ versus $h\nu$ for direct and indirect transitions, respectively, where the band gap was determined by extrapolating the straight-line section with the energy axis. The inset of

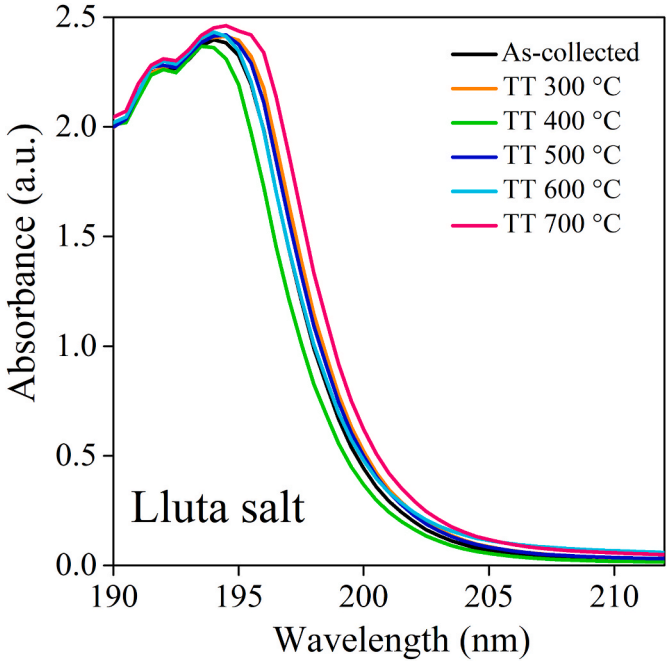

Fig. 13. UV–vis absorption spectra of the Lluta salt samples without and with different AT for 30 min measured in the wavelength range 190–900 nm.

Fig. 14 (a) and (b) shows the variation of the Eg as a function of different thermal annealing. The optical band gap for all samples varies from 6.22 to 6.19, and from 6.09 to 6.00, for direct and indirect transitions, respectively. Addala et al. [54] have found that the synthetic NaCl single crystal produced by the Czochralski method is transparent in the visible region followed by a strong absorption near-ultraviolet region, and with the optical band gap estimated is 6.42 eV [55]. In addition, Messaoudi et al. [56] have calculated the band-gap and phonon distribution in alkali halides by generalized gradient approximation (GGA) and improved by the Engel–Vosko (EV) approximation and the modified Becke–Johnson exchange potential. For NaCl, for instance, they found band gap values of 6.07 and 8.41 for both approximation methods, respectively.

In the present work, although the Eg values vary slightly for different thermal annealing, the maximum and minimum values correspond to that with an AT of 400 and 700 °C for 30 min, respectively. The maximum optical band gap obtained in both cases, direct and indirect transition, corresponds to the sample with an AT of 400 °C, at the same time this sample shows its prominent TL peak at the highest temperature (at about 270 °C) displayed in Fig. 4 at 272 °C. It is related to higher activation energy in the bandgap, that is, the higher energy of the trap activation [42,57]. In other words, the sample with an AT of 400 °C for 30 min presents the higher density of deepest electron traps, which promotes a high-temperature TL peak. This is also related to its higher band gap value found. That is, although the optical band gap value found for this case is slightly greater than the other cases, this is enough to stimulate the appearance of the greatest number of deep traps. In addition, the minimum optical band gap corresponds to a sample with an AT of 700 °C, and at the same time, this sample shows its prominent TL peak at the lowest temperature (at about 161 °C) as shown in Fig. 4. This low-temperature TL peak is related to the lower energy of the trap activation in the band gap of the crystal structure. Namely, although the optical band gap value found for this case is slightly smaller than the other cases, this is enough to stimulate the appearance of the greatest number of shallower traps. Furthermore, for the sample with an AT of 400 °C for 30 min, the calculated activation energy for the prominent computed peak at 269 °C (1.52 eV, vide Table 1) corresponds to about 24.4% of the optical band gap found for this case (6.22 eV, vide Fig. 14 (a)). This indicates that TL peaks with activation energy greater than 24.4% of its optical band gap (for a direct transition) could be considered suitable for use in ionizing radiation dosimetry.

4. Conclusions

Effect of annealing temperature on the structural, thermoluminescence, and optical properties of the thermally treated naturally occurring salt from Lluta and the reliability of using this natural mineral as a retrospective TL dosimeter have been investigated.

The predominant crystalline phase found in Lluta salt sample is NaCl, with minor phases ($CaSO_4$ and Na) accounting for less than 5% of the total. The main peak (002) of the XRD pattern exhibits a shift to lower angles when the thermal annealing on the sample increases indicating an increase of the lattice constant from 5.6449(1) Å to 5.6453(1) Å.

For TL measurements, all samples were irradiated at 2 Gy of gamma dose. Samples show that their prominent TL peak shifts to lower temperatures from 272 to 161 °C when the thermal annealing on the samples increases from 300 to 700 °C for 30 min. Besides, after these AT, an important improvement in the TL intensity is shown. After AT of 400 °C and 600 °C for 30 min, the TL intensity had an increase of about 40 and 80 times the TL intensity of the natural sample, respectively.

Additionally, samples subjected to 400 °C at different times of AT show TL glow curves with a prominent peak at 270 °C for the cases of 30 min and 1h, and a prominent TL peak at 224 °C for the cases from 2 to 24 h. The prominent TL peak, for the case 400 °C for 8 h of AT, shows a high fading which makes its use in dosimetry not possible.

However, TL peak around 270 °C corresponding to the sample with

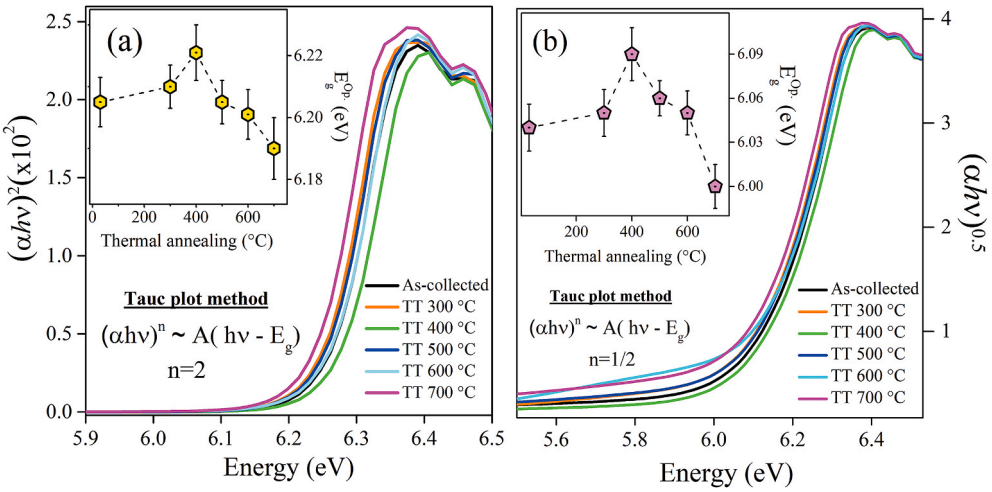

Fig. 14. Optical band gap energy (Eg) of Lluta salt samples at different ATs for (a) direct transition (n = 2) and (b) indirect transition (n = 1/2) band gap. The inset of both subfigures shows the variation of the Eg for different thermal annealing.

an AT of 400 °C for 30 min has a 35% fading in the first 18 days, after that, a constant behavior between about 18 and 39 days has been shown. TL glow curve for this sample, shows four computed TL peaks separated using T_M-Tstop and deconvolution methods at about 120, 216, 269, and 379 °C. Quality of fit was tested with FOM = 2.57%. Furthermore, its prominent TL peak has a linear behavior with a linear equation in the dose range from 50 mGy up to 5 Gy. These results indicate that the salt sample treated in this way has the potential to be used in retrospective dosimetry.

UV–Vis absorption spectra of all samples, both the natural sample and those heat treated, exhibit a broad band between 190 and 205 nm which is attributed to charge transfer transition in the crystal structure. The optical band gap Eg for all samples were calculated using the Tauc relation. Eg values for all samples studied vary from 6.22 to 6.19, and from 6.09 to 6.00, for direct and indirect transitions, respectively. The maximum optical band gap value obtained in both cases, direct and indirect transition, corresponds to the sample with an AT of 400 °C for 30 min, at the same time this sample shows its prominent TL peak at the highest temperature (at about 270 °C). This means that although the optical band gap value found for these cases is slightly greater than the other cases, this increase could be enough to promote the appearance of the greatest number of deep traps.

The lowest optical band gap value found corresponds to that of the sample with an AT of 700 °C for 30 min. Besides, this sample shows its prominent TL peak at the lowest temperature at 161 °C. That is, although the optical band gap value found for this case is slightly smaller than the other cases, this decrease could be enough to promote the appearance of the greatest number of shallower traps.

Finally, for the sample with an AT of 400 °C for 30 min, the calculated activation energy for the prominent computed peak at 269 °C represents about 24.4% of the optical band gap value found for this case.

CRediT authorship contribution statement

Carlos D. Gonzales-Lorenzo: Conceptualization, Methodology, Investigation. **Darwin J. Callo-Escobar:** Methodology, Investigation. **Alberto A. Ccollque-Quispe:** Methodology, Software. **T.K. Gundu Rao:** Methodology, Software, Data curation. **F.F.H. Aragón:** Resources, Investigation, Supervision. **J.C.R. Aquino:** Methodology, Validation, Writing – original draft. **D.G. Pacheco-Salazar:** Writing – original draft, Visualization. **H. Loro:** Writing – review & editing, Resources. **Jose F. Benavente:** Software, Methodology, Validation. **Jessica Mosqueira-Yauri:** Methodology, Validation. **Henry S. Javier-Ccallata:** Methodology, Supervision. **Jorge S. Ayala-Arenas:** Project administration, Funding acquisition. **Nilo F. Cano:** Project administration, Formal analysis.

Declaration of competing interest

The authors declare that they have no known competing financial interests or personal relationships that could have appeared to influence the work reported in this paper.

Acknowledgments

Authors kindly acknowledge the financial support of the project “Consejo Nacional de Ciencia, Tecnología e Innovación Tecnológica (CONCYTEC) - Banco Mundial”, through its executing unit Fondo Nacional de Desarrollo Científico, Tecnológico y de Innovación (FONDECYT), Peru (Process number 037-2019-FONDECYT-BM-INC.INV). Besides, Dr. Hector Loro kindly acknowledges the financial support from FONDECYT, Peru (Conventions 167–168).

References

[1] S.F. Kry, P. Alvarez, J.E. Cygler, L.A. DeWerd, R.M. Howell, S. Meeks, J. O'Daniel, C. Reft, G. Sawakuchi, E.G. Yukihara, AAPM TG 191: clinical use of luminescent dosimeters: TLDs and OSLDs, Med. Phys. 47 (2020) e19–e51.
[2] M. Stabin, M. Tagesson, S. Thomas, M. Ljungberg, S.-E. Strand, Radiation dosimetry in nuclear medicine, Appl. Radiat. Isot. 50 (1999) 73–87.
[3] V. Giurgiutiu, A.N. Zagrai, Use of Smart Materials Technologies in Radiation Environments and Nuclear Industry, Smart Structures and Materials 2000: Smart Structures and Integrated Systems, International Society for Optics and Photonics, 2000, pp. 855–866.
[4] A.P. Møller, T.A. Mousseau, Biological consequences of chernobyl: 20 years on, Trends Ecol. Evol. 21 (2006) 200–207.
[5] Y. Kim, M. Kim, W. Kim, Effect of the Fukushima nuclear disaster on global public acceptance of nuclear energy, Energy Pol. 61 (2013) 822–828.
[6] A. Jaworska, Types of radiation mass casualties and their management, Ann. Ist. Super Sanita 45 (2009) 246–250.
[7] J. Valentin, Protecting People against Radiation Exposure in the Event of a Radiological Attack, SAGE Publications Sage UK, London, England, 2005.
[8] E.R. Svendsen, I. Yamaguchi, T. Tsuda, J.R.D. Guimaraes, M. Tondel, Risk communication strategies: lessons learned from previous disasters with a focus on the Fukushima radiation accident, Curr.Environ. Health Rep. 3 (2016) 348–359.
[9] M. Akselrod, V. Kortov, D. Kravetsky, V. Gotlib, Highly sensitive thermoluminescent anion-defective alpha-Al203: C single crystal detectors, Radiat. Protect. Dosim. 32 (1990) 15–20.
[10] B. Obryk, M. Glaser, I. Mandić, P. Bilski, P. Olko, A. Sas-Bieniarz, Response of various types of lithium fluoride MCP detectors to high and ultra-high thermal neutron doses, Radiat. Meas. 46 (2011) 1882–1885.
[11] J.R. Cameron, N. Suntharalingam, G.N. Kenney, THERMOLUMINESCENT DOSIMETRY, 1968.
[12] J. Roman-Lopez, Y.P. López, E. Cruz-Zaragoza, J. Marcazzó, Optically stimulated luminescence of natural NaCl mineral from Dead Sea exposed to gamma radiation, Appl. Radiat. Isot. 138 (2018) 60–64.

[13] S.N. Singh, A.N. Singh, T.K. Singh, T.R. Singh, Thermoluminescence of natural salt extracted from the saline spring of Ningel, Manipur, Journal ISSN No 2277 (2013) 6362.
[14] M.H. Abdel-wahed, S.M. Abdou, H. Abdel-ghany, H.A. Amer, Thermoluminescence characteristics of NaCl from different origins, J. Sci. Res.Sci. 33 (2016) 201–213.
[15] F.M. Khamis, D. Arafah, Improved thermoluminescence properties of natural NaCl salt extracted from Mediterranean Sea water relevant to radiation dosimetry, Eur. J. Appl. Phys. 2 (2020).
[16] N.B. Wahib, S. Abdul Sani, A. Ramli, S. Ismail, M.H. Abdul Jabar, M.U. Khandaker, E. Daar, K. Almugren, F. Alkallas, D. Bradley, Natural dead sea salt and retrospective dosimetry, Radiat. Environ. Biophys. 59 (2020) 523–537.
[17] A.Y. Shahein, H.S. Hafez, N. Abdou, Retrospective dosimetry using Egyptian halite (NaCl), J. Radiat. Res.Appl. Sci. 12 (2019) 311–318.
[18] S. Druzhyna, H. Datz, Y. Horowitz, L. Oster, I. Orion, Thermoluminescence characteristics of Israeli household salts for retrospective dosimetry in radiological events, Nucl. Instrum. Methods Phys. Res. Sect. B Beam Interact. Mater. Atoms 377 (2016) 67–76.
[19] L. Bøtter-Jensen, S.W. McKeever, A.G. Wintle, Optically Stimulated Luminescence Dosimetry, Elsevier, 2003.
[20] S. Sholom, S. McKeever, Emergency OSL/TL Dosimetry with Integrated Circuits from Mobile Phones, Hard X-Ray, Gamma-Ray, and Neutron Detector Physics XVI, International Society for Optics and Photonics, 2014, p. 921319.
[21] J. Lee, H. Kim, J. Kim, A. Pradhan, M. Kim, I. Chang, S. Lee, B. Kim, C. Park, K. Chung, Thermoluminescence of chip inductors and resistors in new generation mobile phones for retrospective accident dosimetry, Radiat. Meas. 105 (2017) 26–32.
[22] J. Chandler, S. Sholom, S. McKeever, H. Hall, Thermoluminescence and phototransferred thermoluminescence dosimetry on mobile phone protective touchscreen glass, J. Appl. Phys. 126 (2019), 074901.
[23] S. McKeever, S. Sholom, J. Chandler, A comparative study of EPR and TL signals in Gorilla® glass, Radiat. Protect. Dosim. 186 (2019) 65–69.
[24] D. Mesterházy, M. Osvay, A. Kovács, A. Kelemen, Accidental and retrospective dosimetry using TL method, Radiat. Phys. Chem. 81 (2012) 1525–1527.
[25] E. Bortolin, C. Boniglia, S. Della Monaca, R. Gargiulo, S. Onori, P. Fattibene, Is dust a suitable material for retrospective personal dosimetry? Radiat. Meas. 45 (2010) 753–755.
[26] S. Watanabe, N.F. Cano, L.S. Carmo, R.F. Barbosa, J.F. Chubaci, High-and very-high-dose dosimetry using silicate minerals, Radiat. Meas. 72 (2015) 66–69.
[27] I. Bailiff, V. Mikhailik, The use of calcium silicate bricks for retrospective dosimetry, Radiat. Meas. 38 (2004) 91–99.
[28] H. Amer, Development of NaCl salt as a reusable gamma radiation dosimeter, Int. J. Eng.Sci. Invent. (2017) 80–87.
[29] L. Rey, Thermoluminescence of ultra-high dilutions of lithium chloride and sodium chloride, Phys. Stat. Mech. Appl. 323 (2003) 67–74.
[30] K. Murthy, S. Pallavi, G. Rahul, Y. Patel, A. Sai Prasad, D. Elangovan, Thermoluminescence dosimetric characteristics of beta irradiated salt, Radiat. Protect. Dosim. 119 (2006) 350–352.
[31] R. Gartia, B.A. Sharma, U. Ranita, Thermoluminescence Response of Some Common Brands of Iodised Salt, 2004.
[32] K. Ahmad, M.B. Kakakhel, S. Hayat, M. Wazir-ud-Din, M.M. Mahmood, S. U. Rehman, M.T. Siddique, S.M. Mirza, Thermoluminescence study of pellets prepared using NaCl from Khewra Salt Mines in Pakistan, Radiat. Environ. Biophys. 60 (2021) 365–375.
[33] D. Ekendahl, L. Judas, NaCl as a retrospective and accident dosemeter, Radiat. Protect. Dosim. 145 (2011) 36–44.
[34] E.M. Pearce, Kirk-Othmer encyclopedia of chemical technology, J. Polym. Sci., Polym. Lett. Ed. I16 (1978). Wiley-Interscience, New York, 1978, 248-248.
[35] S.R. Feldman, Sodium Chloride, Kirk-Othmer Encyclopedia of Chemical Technology, 2000.
[36] L. De Galan, C. Erkelens, C. Jongerius, W. Maertens, C. Mooring, Determination of traces of impurities in high-purity sodium chloride by differential pulse polarography and flame spectrometry, Fresenius' Z. für Anal. Chem. 264 (1973) 173–176.
[37] P. Sonnenfeld, The color of rock salt—a review, Sediment. Geol. 94 (1995) 267–276.
[38] K.A. Khazal, R.C. Abul-Hail, Study of the possibility of using food salt as a gamma ray dosimeter, Nucl. Instrum. Methods Phys. Res. Sect. A Accel. Spectrom. Detect. Assoc. Equip. 624 (2010) 708–715.
[39] A.C. Larson, R.B. Von Dreele, Gsas, Report lAUR, 1994, pp. 86–748.
[40] J.C. Aquino, F.H. Aragón, J.A. Coaquira, X. Gratens, V.A. Chitta, I. Gonzales, W. A. Macedo, P.C. Morais, Evidence of Cr3+ and Cr4+ coexistence in chromium-doped SnO2 nanoparticles: a structural and magnetic study, J. Phys. Chem. C 121 (2017) 21670–21677.
[41] D E G (Ed.), American Institute of Physics Handbook, McGrawHill, New York, 1972.
[42] S. Mckeever, Thermoluminescence of Solids, Cambridge University Press, London New York, 1985.
[43] R. Chen, S.W.S. McKeever, Theory of Thermoluminescence and Related Phenomena, World Scientific, 1997.
[44] S.W.S. McKeever, On the analysis of complex thermoluminescence. Glow-curves: resolution into individual peaks, physica status solidi (a) 62 (1980) 331–340.
[45] J. Benavente, J. Gómez-Ros, A. Romero, Thermoluminescence glow curve deconvolution for discrete and continuous trap distributions, Appl. Radiat. Isot. 153 (2019) 108843.
[46] P. Kivits, H.J.L. Hagebeuk, Evaluation of the model for thermally stimulated luminescence and conductivity; reliability of trap depth determinations, J. Lumin. 15 (1977) 1–27.
[47] H.G. Balian, N.W. Eddy, Figure-of-merit (FOM), an improved criterion over the normalized chi-squared test for assessing goodness-of-fit of gamma-ray spectral peaks, Nucl. Instrum. Methods 145 (1977) 389–395.
[48] G. Kitis, J.M. Gomez-Ros, J.W.N. Tuyn, Thermoluminescence glow-curve deconvolution functions for first, second and general orders of kinetics, J. Phys. Appl. Phys. 31 (1998) 2636.
[49] C. Gopikrishnan, D. Jose, A. Datta, Electronic structure, lattice energies and Born exponents for alkali halides from first principles, AIP Adv. 2 (2012), 012131.
[50] F. Abeles, Optical Properties of Solids, 1972.
[51] H. Nagabhushana, B. Nagabhushana, M.M. Kumar, K. Murthy, C. Shivakumara, R. Chakradhar, Synthesis, characterization and photoluminescence properties of CaSiO3: Eu3+ red phosphor, Spectrochim. Acta Mol. Biomol. Spectrosc. 78 (2011) 64–69.
[52] K.K. Kumar, Y. Pavani, M. Ravi, S. Bhavani, A. Sharma, V.N. Rao, Effect of complexation of NaCl salt with polymer blend (PEO/PVP) electrolytes on ionic conductivity and optical energy band gaps, in: AIP Conference Proceedings, American Institute of Physics, 2011, pp. 641–644.
[53] A.A.A. Ahmed, A.M. Al-Hussam, A.M. Abdulwahab, A.N.A.A. Ahmed, The impact of sodium chloride as dopant on optical and electrical properties of polyvinyl alcohol, AIMS.Mater. Sci. 5 (2018) 533–542.
[54] S. Addala, L. Bouhdjer, A. Chala, A. Bouhdjar, O. Halimi, B. Boudine, M. Sebais, Structural and optical properties of a NaCl single crystal doped with CuO nanocrystals, Chin. Phys. B 22 (2013), 098103.
[55] A. Othmani, J. Plenet, E. Berstein, C. Bovier, J. Dumas, P. Riblet, P. Gilliot, R. Levy, J. Grun, Nanocrystals of CdS dispersed in a sol-gel silica glass: optical properties, J. Cryst. Growth 144 (1994) 141–149.
[56] I. Messaoudi, A. Zaoui, M. Ferhat, Band-gap and phonon distribution in alkali halides, physica status solidi (b) 252 (2015) 490–495.
[57] C.D. Gonzales-Lorenzo, T.G. Rao, N.F. Cano, B.N. Silva-Carrera, R.R. Rocca, E. E. Cuevas-Arizaca, J.S. Ayala-Arenas, S. Watanabe, Thermoluminescence and defect centers in β-CaSiO3 polycrystal, J. Lumin. 217 (2020) 116783.